# Saturated STA-based sliding-mode tracking control of AUVs: Design, stability analysis, and experiments

Jesús Guerrero, Ahmed Chemori, Vincent Creuze, Jorge Torres, Eduardo Campos

# Highlights

## Saturated STA-based sliding-mode tracking control of AUVs: Design, stability analysis, and experiments

Jesús Guerrero,Ahmed Chemori,Vincent Creuze,Jorge Torres,Eduardo Campos

- A saturated super-twisting algorithm is proposed for autonomous underwater vehicles.
- Lyapunov-based stability analysis of the resulting closed-loop system is performed.
- Real-time experiments demonstrate the effectiveness and robustness of the algorithm.

# Saturated STA-based sliding-mode tracking control of AUVs: Design, stability analysis, and experiments

Jesús Guerrero[a,1], Ahmed Chemori[b,*], Vincent Creuze[b], Jorge Torres[c] and Eduardo Campos[d]

[a]Mechatronics Department, Tecnológico Nacional de México / ITS Abasolo, México
[b]LIRMM, University of Montpellier, CNRS, Montpellier, France
[c]Center for Research and Advanced Studies of the National Polytechnic Institute (CINVESTAV), Mexico city, México
[d]CONACYT-Universidad del Istmo, Santo Domingo Tehuantepec, Oaxaca, México

ARTICLE INFO

*Keywords*:
Robust control
Super-Twisting Algorithm
AUV
Stability analysis
Real-time experiments

ABSTRACT

In this study, we developed a saturated super-twisting algorithm for autonomous underwater vehicles to address the trajectory tracking problem. On the basis of Lyapunov arguments, we performed a stability analysis of the resulting closed-loop system under the proposed controller, considering the MIMO system dynamics, parametric uncertainties, and external disturbances. Finally, we conducted several real-time experiments to demonstrate the effectiveness and robustness of the proposed control solution as compared to the traditional super-twisting algorithm.

## 1. Introduction and related work

Autonomous underwater vehicles (AUVs) have become increasingly popular in recent years owing to their ability to perform various tasks in underwater environments. However, designing a controller that can maintain the AUV at a specific point or ensure the tracking of the desired trajectory is a challenging task Tijjani, Chemori, Ali and Creuze (2022a). The nonlinearity, random external disturbances, and difficulty in accurately modeling hydrodynamic effects hinder the design of an efficient controller. Therefore, various control schemes have been proposed in the literature, such as proportional–derivative (PD)/proportional—integral–derivative (PID) control Herman (2009); Sarhadi, Noei and Khosravi (2016), their adaptive and improved versions Campos, Chemori, Creuze, Torres and Lozano (2017); Guerrero, Torres, Creuze, Chemori and Campos (2019b); Liu, Zhang, Pan and Zhang (2022), neural network feedback linearization Shojaei (2022), model predictive control Yan, Gong, Zhang and Wu (2020); Yan, Yan, Cai, Yu and Wu (2023), fuzzy controllers Xiang, Yu, Lapierre, Zhang and Zhang (2018), adaptive control Maalouf, Creuze and Chemori (2012); Quiao and Zhang (2019); Zhong, Yu, Wang, Liu, and Lian (2022); Li, Wen, Cao, Yao, Lian and Mao (2023), and other techniques Xu, Haroutunian, Murphy, Neasham and Norman (2020); Tijjani, Chemori and Creuze (2022b). However, new methods to improve the control performance of these vehicles have been extensively explored.

The control of AUVs is a critical field, and sliding-mode control (SMC) techniques have emerged as key solutions owing to their ability to ensure robustness against parametric uncertainties and external disturbances Tijjani, Chemori and Creuze (2020). However, first-order SMC schemes exhibit a drawback, namely, chattering due to high-frequency switching in control signals. To address this issue, high-order sliding-mode controllers (HOSMCs) have been developed as enhanced alternatives for mitigating chattering effects.

One notable HOSMC scheme is the super-twisting algorithm (STA) Levant (1993). The STA have been successfully applied to control underwater robots Guerrero, Torres, Antonio and Campos (2018); Guerrero, Torres, Creuze and Chemori (2019a); Manzanilla, Ibarra, Salazar, Zamora, Lozano and Munoz (2021); Guerrero, Torres, Creuze and Chemori (2023); Li, Gao, Huang and Yang (2024). The STA can be regarded as similar to a nonlinear proportional–integral (PI) controller; it retains the favorable properties of the first-order SMC while suppressing chattering.

However, the integral part of the STA introduces challenges that are reminiscent of the windup effect observed in traditional PI controllers. This issue was addressed in a prior study Seeber and Reichhartinger (2020) wherein a modified STA control law was proposed by employing a conditioning technique to mitigate the windup in an SMC system. The closed-loop stability was rigorously analyzed, considering bounded Lipschitz continuous perturbations, and the efficacy of the controller was demonstrated through numerical simulations and real-time experiments with a servomotor.

Similarly, Castillo, Steinberger, Fridman, Moreno and Horn (2021) proposed a saturated super-twisting algorithm with structures that dynamically switched between a relay controller and an STA. This switching is governed by a Lyapunov-based law that allows for the generation of bounded control signals.

Golkani, Koch, Reichhartinger and Horn (2018) employed a unique approach and focused on an STA-based feedback control law to regulate a first-order system under disturbances. They demonstrated global finite-time stability

*Corresponding author
jesus.gt@abasolo.tecnm.mx (J. Guerrero); Ahmed.Chemori@lirmm.fr (A. Chemori); vincent.creuze@lirmm.fr (V. Creuze); jtorres@ctrl.cinvestav.mx (J. Torres); ecampos@conacyt.mx (E. Campos)
https://jnguerrero.github.io/ (J. Guerrero)
ORCID(s): 0000-0002-5873-8986 (J. Guerrero); 0000-0001-9739-9473 (A. Chemori)

through numerical simulations; however, they acknowledged limitations in applicability to other control algorithms or more complex higher-order systems. Further, they did not present real-time experimental results.

This study first entailed a review that highlights the evolution of SMC techniques, particularly HOSMCs such as STA, and the ongoing efforts to address the associated challenges. In this context, a saturated super-twisting algorithm for AUV trajectory tracking was designed.

This study makes several remarkable contributions. The prior study Golkani, Koch, Reichhartinger and Horn (2018), wherein they developed a saturated super-twisting controller for the stabilization of a scalar system, formed the basis of this study. We extended their results to a multiple-input and multiple-output (MIMO) AUV. Moreover, we addressed the trajectory tracking problem. Stability analysis of the resulting closed-loop system was performed using the Lyapunov approach. The effectiveness and robustness of the proposed controller were demonstrated through real-time experiments, and a comparative study was performed with a nominal STA controller.

The remainder of this paper is organized as follows. The mathematical modeling of underwater vehicles is presented in Section 2. The design of the proposed robust disturbance observer based on the STA is detailed in Section 3, and a stability analysis of the proposed observer is presented in Section 4. Section 5 introduces the nominal PD controller, which is enhanced by the proposed disturbance observer, and its stability analysis. The real-time experiments, conducted on a real platform, to demonstrate the effectiveness and robustness of the proposed methodology are described in Section 6. Finally, Section 7 summarizes the concluding remarks.

## 2. Mathematical model of the AUV

Mathematical models of underwater vehicles have been reported in several studies Fossen (1999, 2011); Sarhadi, Noei and Khosravi (2016). The resulting dynamic model in terms of the body-fixed frame is as follows:

$$M\dot{\nu} + C(\nu)\nu + D(\nu)\nu + g(\eta) = \tau + w_{\nu}(t) \quad (1)$$

$$\dot{\eta} = J(\eta)\nu \quad (2)$$

Here, $\nu \in \mathbb{R}^6$ denotes the state vector of velocity relative to the body-fixed frame, $M \in \mathbb{R}^{6\times6}$ is the inertia matrix, $C(\nu) \in \mathbb{R}^{6\times6}$ represents the Coriolis-centripetal matrix, $D(\nu) \in \mathbb{R}^{6\times6}$ is the hydrodynamic damping matrix, $g(\cdot) \in \mathbb{R}^6$ represents the vector of gravitational and buoyancy forces and moments, $\tau$ is the control vector acting on the vehicle, and $w_{\nu}(t)$ represents the vector containing the effects of external disturbances.

Using Eq. (2) and the transformation matrix $J(\eta) \in \mathbb{R}^{6\times6}$, the dynamics of the underwater vehicle can be expressed in the earth-fixed frame as illustrated in Figure 1. The vector $\eta = [x, y, z, \phi, \theta, \psi]^T$ represents the position and orientation of the vehicle in the earth-fixed frame, and $\dot{\eta}$ is its time derivative. The resulting representation in the earth-fixed frame is expressed as follows:

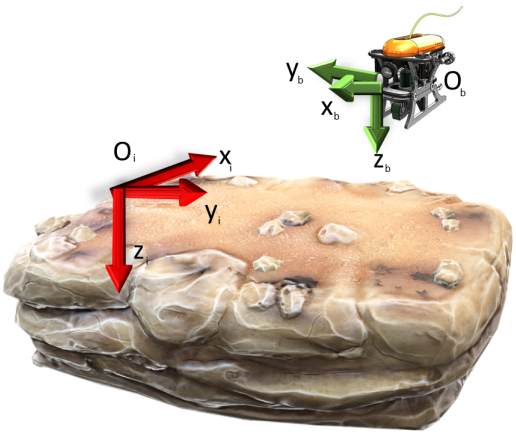


**Figure 1:** Illustration of the earth-fixed frame $(O_i, x_i, y_i, z_i)$ and the body-fixed frame $(O_b, x_b, y_b, z_b)$.

$$M_{\eta}(\eta)\ddot{\eta} + C_{\eta}(\nu,\eta)\dot{\eta} + D_{\eta}(\nu,\eta)\dot{\eta} + g_{\eta}(\eta) = \tau_{\eta}(\eta) + \overline{w}_{\eta}(t) \quad (3)$$

where the individual terms are defined as follows:

$$\begin{aligned}
M_{\eta}(\eta) &= J^{-T}(\eta) M J^{-1}(\eta) \\
C_{\eta}(\nu,\eta) &= J^{-T}(\eta)\left[C(\nu) - M J^{-1}(\eta)\dot{J}(\eta)\right] J^{-1}(\eta) \\
D_{\eta}(\nu,\eta) &= J^{-T}(\eta) D(\nu) J^{-1}(\eta) \\
g_{\eta}(\eta) &= J^{-T}(\eta) g(\eta) \\
\tau_{\eta}(\eta) &= J^{-T}(\eta)\tau \\
\overline{w}_{\eta}(t) &= J^{-T}(\eta) w_{\nu}(t)
\end{aligned}$$

These terms represent the matrices of the dynamic model, while $\overline{w}_{\eta}(t)$ denotes the vector containing the effects of external disturbances.

As accurately estimating the hydrodynamic parameters of a vehicle is difficult, the dynamics of the vehicle are expressed in terms of the estimated parameters as follows:

$$\hat{M}_{\eta}(\eta)\ddot{\eta} + \hat{C}_{\eta}(\nu,\eta)\dot{\eta} + \hat{D}_{\eta}(\nu,\eta)\dot{\eta} + \hat{g}_{\eta}(\eta) = \tau_{\eta}(\eta) + w_{\eta}(t) \quad (4)$$

where $\hat{M}_{\eta}$, $\hat{C}_{\eta}$, $\hat{D}_{\eta}$, and $\hat{g}_{\eta}$ represent the estimations of the matrices of the dynamic model. The vector $w_{\eta}(t)$ includes the effects of external disturbances and unknown dynamics of the vehicle. This can be defined as follows:

$$w_{\eta}(t) = \overline{w}_{\eta} - \tilde{f}(\cdot) \quad (5)$$

Here, $\tilde{f}(\cdot)$ represents the unknown dynamics of the model, and it is expressed as follows:

$$\tilde{f}(\cdot) = (M_{\eta} - \hat{M}_{\eta})\ddot{\eta} + (C - \hat{C}\eta)\dot{\eta} + (D - \hat{D}_{\eta})\dot{\eta} + (g_{\eta} - \hat{g}_{\eta}) \quad (6)$$

## 3. Proposed control scheme design

This section details the design of the saturated super-twisting algorithm (hereinafter referred to as Sat-STA) for the trajectory tracking of AUVs. The proposed methodology is based on a prior study Golkani, Koch, Reichhartinger and Horn (2018) that entailed the development of a novel saturated STA to improve the nominal algorithm by considering the saturation in the control input.

Golkani, Koch, Reichhartinger and Horn (2018) proposed a saturated controller for a scalar nonlinear system. However, in the case considered in this study, the AUV dynamics given by (4) represent a MIMO system. Therefore, before designing a control law, the dynamic model must be reformulated to provide a more comprehensive description of the proposed control scheme. To this end, we considered the following state variables:

$$z_1 = \eta \quad ; \quad z_2 = \dot{\eta}$$

Then, the dynamic model (4) can be expressed as a control affine structure as follows:

$$\begin{aligned} \dot{z}_1 &= z_2 \\ \dot{z}_2 &= \hat{F}(z) + \hat{G}(z)u(t) + d(t) \end{aligned} \tag{7}$$

where the terms involved in (7) are given by

$$\begin{aligned} \hat{F}(z) &= -\hat{M}_\eta(\eta)^{-1}\left[\hat{C}_\eta(\nu,\eta)\dot{\eta} + \hat{D}_\eta(\nu,\eta)\dot{\eta} + \hat{g}_\eta(\eta)\right] \\ \hat{G}(z) &= \hat{M}_\eta(\eta)^{-1}J^{-T}(\eta) \\ d(t) &= \hat{M}_\eta(\eta)^{-1}w_\eta(t) \\ u(t) &= \tau_\eta \end{aligned}$$

The following assumptions are made:

**Assumption 1**. The pitch angle is smaller than $\pi/2$, that is, $|\theta| < \pi/2$.

**Assumption 2**. The perturbation term $w(t)$ is a Lipschitz continuous function.

Assumption A1 ensures that the inverse of the matrix $J(\eta)$ always exists; consequently, the term $G(z)$ also exists. A pitch close to $\pi/2$ implies that the robot dives vertically; this is generally not required during standard remotely operated vehicle (ROV) operation.

Assumption A2 ensures that the time derivative of the considered disturbance is bounded, that is,

$$|\dot{d}_i(t,x)| \leq L_i, \qquad i = \overline{1,6}. \tag{8}$$

with $L_i \geq 0$. From a practical perspective, the external disturbances are always bounded.

From the dynamic model (7), we propose a sliding surface $\sigma(t)$, which depends on the tracking error $e(t)$ as follows:

$$\sigma(t) = \dot{e}(t) + \Gamma e(t) \tag{9}$$

where $\sigma = [\sigma_1, \sigma_2, \cdots, \sigma_6]^T$. Further, $e(t) = \eta_d - \eta = z_1^d - z_1$ is the tracking error vector, and the desired trajectory is defined as $\eta_d = z_1^d(t) = [x_d(t), y_d(t), z_d(t), \phi_d(t), \theta_d(t), \psi_d(t)]^T$. In addition, the time derivative of the tracking error is expressed as $\dot{e}(t)$, and $\Gamma = diag\{\gamma_1, \gamma_2, \cdots, \gamma_6\}$ is a diagonal positive definite matrix.

We propose the following control law for underwater vehicles:

$$u(t) = \hat{G}(z)^{-1}\left[\ddot{z}_1^d + \Gamma\dot{e}(t) - \hat{F}(z) - u_{sat}\right] \tag{10}$$

where $u_{sat}$ is the Sat-STA defined as

$$u_{sat} = -K_1 \mathrm{SAT}_\delta\left(\mathrm{ABS}^{1/2}(\sigma)\right)\mathrm{SGN}(\sigma)^T + \Lambda \tag{11}$$

$$\dot{\Lambda} = -K_2\mathrm{SGN}(\sigma) - K_3\Lambda \tag{12}$$

with the following definitions of shorthand notation used:

$$\mathrm{ABS}^{1/2}(\sigma) = \mathrm{diag}\left(\sqrt{|\sigma_1|}, \sqrt{|\sigma_2|}, \ldots, \sqrt{|\sigma_6|}\right)$$

$$\mathrm{SAT}_\delta\left(\mathrm{ABS}^{1/2}(\sigma)\right) = \mathrm{diag}\left(sat_{\delta_1}(\sqrt{|\sigma_1|}), ..., sat_{\delta_6}(\sqrt{|\sigma_6|})\right)$$

$$\mathrm{SGN}(\sigma) = \left[sgn(\sigma_1), sgn(\sigma_2), \ldots, sgn(\sigma_n)\right]^T$$

The feedback control gains are positive definite matrices satisfying $K_j = K_j^T > 0$ for $j = 1, 2, 3$, and they are explicitly defined as $K_i = \mathrm{diag}\{k_{i,1}, k_{i,2}, \cdots, k_{i,6}\} > 0$ for $i = 1, 2, 3$. The time derivative of the vector $\Lambda = [\lambda_1, \lambda_2, \cdots, \lambda_6]^T$ is denoted by $\dot{\Lambda}$. The function $sgn(\cdot)$ represents the sign function. The saturation function $\mathrm{sat}_\delta(\cdot)$ is defined as

$$\mathrm{sat}_\delta(q) = \begin{cases} q & \text{for } |q| < \delta \\ \delta\mathrm{sgn}(q) & \text{for } |q| \geq \delta \end{cases} \tag{13}$$

The following condition on this function always holds:

$$0 \leq \mathrm{sat}_\delta(|q|^{\frac{1}{2}}) \leq \delta, \quad \forall q \tag{14}$$

where $q$ denotes an auxiliary variable.

Finally, by selecting the positive feedback control gains, for any initial condition of $\sigma_i(0)$, the sliding surface $\sigma_i = 0$ is reached in a finite time, and the continuous actuation signal remains simultaneously in a bounded vicinity.

## 4. Closed-loop stability analysis

**Theorem 1.** *Consider the underwater vehicle dynamic model (7), and suppose that the disturbance term is upper-bounded by (8). Then, for any initial condition $z(0), \sigma(0)$, the sliding surface $\sigma = 0$ is reached in a finite time under the Sat-STA (10).*

PROOF. First, consider the sliding surface given by (9). By computing the time derivative of this sliding surface and substituting it into the proposed control law, we obtain the following closed-loop error dynamics:

$$\dot{\sigma} = -K_1\mathrm{SAT}_\delta(\sigma)\mathrm{SGN}(\sigma)^T + \Lambda + w(t) \tag{15}$$

Now, the following changes in the variables are considered:

$$s_{1i} = \sigma_i \tag{16}$$

$$s_{2i} = \Lambda_i + w_i(t) \tag{17}$$

Then, by taking the time derivative of (16)–(17) and employing (39), the dynamics of the sliding surface (15) can be rewritten in scalar form ($i = \overline{1,6}$) as follows:

$$\begin{aligned}\dot{s}_{1i} &= -k_{1i}\text{sat}(|s_{1i}|^{\frac{1}{2}})sgn(s_{1i}) + s_{2i}\\ \dot{s}_{2i} &= -k_{2i}sgn(s_{1i}) - k_{3i}s_{2i} + \rho_i(t)\end{aligned}$$

where $\rho_i(t) = k_{3i}w_i(t) + \dfrac{d}{dt}w_i(t)$.

Without loss of generality, the system can be represented using the following simplified notation:

$$\begin{aligned}\dot{s}_1 &= -k_1\text{sat}(|s_1|^{\frac{1}{2}})sgn(s_1) + s_2\\ \dot{s}_2 &= -k_2sgn(s_1) - k_3s_2 + \rho(t)\end{aligned} \tag{18}$$

Given the transformed dynamics of $\sigma$, two cases can be distinguished: (i) an unperturbed system, and (ii) a perturbed system, both of which were analyzed in this study.

*I. Unperturbed system:*

In this case, we consider that the dynamic system (18) is not subjected to external disturbances. This implies that $w(t) = 0$, and, therefore, $\rho(t) = 0$. Consequently, the dynamic system is expressed as follows:

$$\begin{aligned}\dot{s}_1 &= -k_1\text{sat}(|s_1|^{\frac{1}{2}})sgn(s_1) + s_2\\ \dot{s}_2 &= -k_2sgn(s_1) - k_3s_2\end{aligned} \tag{19}$$

Consider the following Lyapunov candidate function:

$$V = \xi^T P_1 \xi \tag{20}$$

where the vector $\xi$ is defined by $\xi = [|s_1|^{\frac{1}{2}}\text{sgn}(s_1)\ \ s_2]^T$, and the matrix P is given by

$$P_1 = \frac{1}{2}\begin{bmatrix}2 & 0\\ 0 & \frac{1}{k_2}\end{bmatrix} \tag{21}$$

$V$ is a positively definite and radially unbounded function. Then, taking the time derivative of $V$, we obtain

$$\dot{V} = 2\xi^T P_1 \dot{\xi} \tag{22}$$

$$= -k_1\text{sat}_\delta(|s_1|^{\frac{1}{2}}) - \frac{k_3}{k_2}s_2^2 \tag{23}$$

If the constant feedback control gains are positive, $\dot{V}$ is negatively definite. Thus, in this case, the origin $\sigma = 0$ is globally asymptotically stable. Moreover, following the arguments by Golkani, Koch, Reichhartinger and Horn (2018) and invoking Lemma 2 and Theorem 4.2 by Orlov (2008), because the continuous function $\psi = -k_3s_2 + \rho(t)$ of the inhomogeneous system (18) is bounded, the conditions of the quasihomogeneity principle are fulfilled. Therefore, the convergence of vector $\xi$ in finite time is ensured by applying the aforementioned principle. Finally, it can be concluded that the closed-loop system converges to the origin in finite time.

*II. Perturbed system:*

In this case, an external disturbance is considered, implying that $w(t) \neq 0$ and, consequently, $\rho(t) \neq 0$.

To prove the stability in this case, we consider the Lyapunov candidate function Golkani, Koch, Reichhartinger and Horn (2018), defined as

$$V = \xi^T P_1 \xi + \varsigma^T P_2 \varsigma \tag{24}$$

where $\varsigma = [s_1 \quad s_2]^T$, and the matrices $P_1$ and $P_2$ are defined as

$$P_1 = \frac{1}{2}\begin{bmatrix}k_1^2 + 6k_2 & -k_1\\ -k_1 & 1\end{bmatrix}, \quad P_2 = \frac{1}{2}\begin{bmatrix}k_3^2 & k_3\\ k_3 & 2\end{bmatrix} \tag{25}$$

Notably, (24) is continuous everywhere and continuously differentiable except at the origin.

Computing the time derivative of $V$ along the trajectories of the system dynamics (19) yields

$$\begin{aligned}\dot{V} \quad &= -\tfrac{1}{2}k_1(6k_2 + k_1^2)\text{sat}(\cdot) + \frac{k_1^2}{2|s_1|^{\frac{1}{2}}}\text{sat}(\cdot)\text{sgn}(s_1)s_2\\ &\quad -k_1k_3^2s_1\text{sat}(\cdot)\text{sgn}(s_1) - k_1k_3\text{sat}(\cdot)\text{sgn}(s_1)s_2\\ &\quad \tfrac{1}{2}(6k_2 + k_1^2)\text{sgn}(s_1)s_2 - \frac{k_1}{|s_1|^{\frac{1}{2}}}s_2^2 - 2k_3s_2^2\\ &\quad +k_1k_2|s_1|^{\frac{1}{2}} + k_1k_3|s_1|^{\frac{1}{2}}\text{sgn}(s_1)s_2 - k_1|s_1|^{\frac{1}{2}}\text{sgn}(s_1)\rho(t)\\ &\quad -3k_2\text{sgn}(s_1)s_2 + 3s_2\rho(t) - k_2k_3s_1\text{sgn}(s_1) + k_3s_1\rho(t)\end{aligned} \tag{26}$$

where $\text{sat}(\cdot) = \text{sat}(|s_1|^{\frac{1}{2}})$.

Moreover, the saturation function explicitly appears in the dynamics of $\dot{V}$. To comprehensively explain the stability analysis, we considered the following two cases:

**Case 1.** $|s_1|^{\frac{1}{2}} < \epsilon$.

In this case, the time derivative of $V$ along the system trajectories is as follows:

$$\begin{aligned}\dot{V} = &-\Big(2k_1k_2 + \frac{k_1^3}{2}\Big)|s_1|^{\frac{1}{2}} + k_1^2s_2sgn(s_1) - \frac{k_1s_2^2}{2|s_1|^{\frac{1}{2}}} +\\ &+ 3s_2\rho(t) - k_1|s_1|^{\frac{1}{2}}\text{sgn}(s_1)\rho(t) + k_3s_1\rho(t) -\\ &- k_1k_3^2|s_1|^{\frac{3}{2}} - 2k_3s_2^2 - k_2k_3|s_1|\end{aligned} \tag{27}$$

Then, considering that the perturbation is upper-bounded, as in (8), the time derivative of $V$ can be expressed as

$$\dot{V} \leq -\frac{1}{|s_1|^{\frac{1}{2}}}\xi^T Q_1 \xi - k_1k_3^2|s_1|^{\frac{3}{2}} - 2k_3s_2^2 - k_3(k_2 - L_M)|s_1| \tag{28}$$

where the matrix $Q$ is defined as follows:

$$Q_1 = \frac{1}{2}\begin{bmatrix}4k_1k_2 + k_1^3 - 2k_1L_M & -(k_1^2 + 3L_M)\\ -(k_1^2 + 3L_M) & k_1\end{bmatrix}.$$

Now, we select different parameters in $Q_1$ as follows Golkani, Koch, Reichhartinger and Horn (2018):

$$k_1 > 0,\ k_3 > 0,\ k_2 > 4L_M + \frac{9L_M^2}{2k_1^2} + \frac{k_1^2}{2},\ \epsilon > \frac{k_2}{k_3^2} + \frac{2k_2}{6k_2 + k_1^2} \tag{29}$$

Then, the matrix $Q$ is positive definite. Consequently, the time derivative of $V$ is negative definite.

**Case 2.** $|s_1|^{\frac{1}{2}} \geq \epsilon$.

In this case, the time derivative of $V$ leads to the following:

$$\begin{aligned}\dot{V} = &-\epsilon k_1\Big(3k_2 + \frac{k_1^2}{2}\Big) + \Big(\frac{k_1^2}{2} - \epsilon k_1 k_3\Big)s_2\mathrm{sgn}(s_1) - \\ &- \frac{k_1 s_2^2}{2|s_1|^{\frac{1}{2}}} + k_1 k_2|s_1|^{\frac{1}{2}} + 3s_2\rho(t) - k_1|s_1|^{\frac{1}{2}}\mathrm{sgn}(s_1)\rho(t) \\ &- \Big(\epsilon k_1 k_3^2 + k_2 k_3\Big)|s_1| - 2k_3 s_2^2 + k_3 s_1\rho(t) + \\ &+ k_1 k_3 s_2|s_1|^{\frac{1}{2}}\mathrm{sgn}(s_1) + \frac{\epsilon k_1^2}{2}\frac{s_2\mathrm{sgn}(s_1)}{|s_1|^{\frac{1}{2}}}\end{aligned} \tag{30}$$

We now consider the following inequalities from the literature Golkani, Koch, Reichhartinger and Horn (2018):

$$-\epsilon k_1 k_3 s_2\mathrm{sgn}(s_1) \leq -k_1 k_3 s_2|s_1|^{\frac{1}{2}}\mathrm{sgn}(s_1) \tag{31}$$

$$\frac{\epsilon k_1^2}{2}\frac{s_2\mathrm{sgn}(s_1)}{|s_1|^{\frac{1}{2}}} \leq \frac{k_1^2}{2}s_2\mathrm{sgn}(s_1) \tag{32}$$

The time derivative of the Lyapunov function, $\dot{V}$, can be expressed as follows:

$$\begin{aligned}\dot{V} \leq &-\frac{1}{|s_1|^{\frac{1}{2}}}\xi^T Q_2\xi - \epsilon k_1\Big(3k_2 + \frac{k_1^2}{2}\Big) - 2k_3 s_2^2 - \\ &- k_3(k_2 - L_M)|s_1| + 2k_1 k_2|s_1|^{\frac{1}{2}} - \epsilon k_1 k_3^2|s_1|\end{aligned} \tag{33}$$

where the matrix $Q_2$ is defined as

$$Q_2 = \frac{1}{2}\begin{bmatrix} 2k_1k_2 - 2k_1L_M & -(k_1^2 + 3L_M) \\ -(k_1^2 + 3L_M) & k_1 \end{bmatrix}. \tag{34}$$

The fifth element on the right-hand side of (33) can be rewritten using Young's inequality as follows:

$$2k_1 k_2|s_1|^{\frac{1}{2}} \leq k_1 k_2(|s_1| + 1) \tag{35}$$

Consequently, $\dot{V}$ can be simplified as

$$\begin{aligned}\dot{V} \leq &-\frac{1}{|s_1|^{\frac{1}{2}}}\xi^T Q_2\xi - \epsilon k_1\Big(3k_2 + \frac{k_1^2}{2} - \frac{k_2}{\epsilon}\Big) - 2k_3 s_2^2 - \\ &- \Big(k_3(k_2 - L_M) + k_1(\epsilon k_3^2 - k_2)\Big)|s_1|\end{aligned} \tag{36}$$

Considering the conditions (29), $\dot{V}$ can be ensured to be negative definite, and global asymptotic convergence is achieved. Following the same arguments as in the unperturbed case and invoking Theorem 4.2 by Orlov (2008), because the continuous function $\psi = -k_3 s_2 + \rho(t)$ of the inhomogeneous system (18) is bounded, the conditions of the quasihomogeneity principle are fulfilled. Therefore, the convergence of the vector $\xi$ in a finite time is ensured by applying the aforementioned principle. Finally, it can be concluded that the closed-loop system converges to the origin in a finite time.

This implies that $s_i = 0$, and the sliding surface then approaches zero (i.e., $\sigma \to 0$) according to (16). Considering (9), this implies that $\lim_{t\to\infty} e(t) = 0$ and $\lim_{t\to\infty} \dot{e}(t) = 0$; thus, $\eta_d \to \eta$ asymptotically.

## 5. Real-time experimental results

The experiments were performed to validate the proposed control scheme for a Leonard underwater vehicle, designed at the LIRMM research laboratory, France. The Leonard ROV is a tethered vehicle measuring 75 cm × 55 cm × 45 cm and weighing 28 kg, with six thrusters to activate its six DOFs. For this purpose, a laptop with a 2.9 GHz Intel Core i7-3520M CPU and 8 GB of RAM, with Windows 10 OS and Visual C++ 2015, serves as the data processing and control unit. This computer receives data in real time from the vehicle's sensors, including the depth sensor and inertial measurement unit (IMU), uses them to calculate control actions, and sends them to the actuators controlled by Syren 10 motor drivers. The vehicle had a sampling period of 50 ms, and the measurement latency was less than 5 ms, which can be neglected, particularly for the slow dynamics of underwater vehicles. The main features of the Leonard ROV are summarized in Table 1.

The experiments were conducted in a 4 m × 3 m × 2 m pool in the LIRMM laboratory, as shown in Figure 2. The proposed saturated control scheme (10) was designed for the six degrees of freedom (DOFs) of the vehicle; however, the experiments focused on two DOFs, namely, the depth (translation) and yaw (rotation). The control objective is to robustly track the desired trajectory in depth and yaw dynamics, in the presence of uncertainties and external disturbances. A general flowchart for the implementation of the proposed controller is presented in Fig. 3.

The results clearly indicate that the proposed control algorithm effectively controls the Leonard ROV. This is described in the following subsection.

### 5.1. Comparison with other controllers

To demonstrate the advantages of the proposed saturated controller (10), we compared it with other popular techniques, such as the STA controller wherein the control law is defined as

$$u(t) = \hat{G}(z)^{-1}\Big[\ddot{z}_1^d + \Lambda\dot{e}(t) - \hat{F}(z) - u_{STA}\Big] \tag{37}$$


**Figure 2:** Workstation for the real-time experiments; the Leonard robot and the experimental setup are shown.

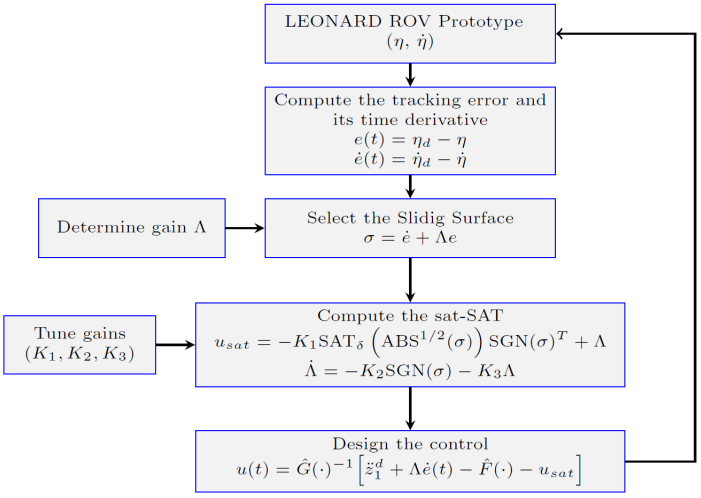


**Figure 3:** Flowchart of the implementation of the controller.

where $u_{STA}$ is the nominal STA, defined as

$$u_{STA} = -K_1 \mathrm{ABS}^{1/2}(\sigma)\mathrm{SGN}(\sigma)^T + \Lambda \tag{38}$$

$$\dot{\Lambda} = -K_2 \mathrm{SGN}(\sigma) \tag{39}$$

where the controller feedback gains $K_1$ and $K_2$ are diagonal and positive definite matrices, respectively, and are equal to the corresponding values found for the Sat-STA control.
Furthermore, we compared our approach with an adaptive version of the STA. Guerrero, Torres, Creuze and Chemori (2019a) proposed an adaptive generalized super-twisting algorithm. In their control law, the design parameters are chosen such that $\mu_{1i} = 1$ and $\mu_{2i} = 0$; thus, it is possible to recover the nominal STA proposed in (38). Hence, the adaptive controller feedback gains $K_1 = \mathrm{diag}\left(k_{1,1}, k_{1,2}, \cdots, k_{1,6}\right)$ and $K_2 = \mathrm{diag}\left(k_{2,1}, k_{2,2}, \cdots, k_{2,6}\right)$ can be constructed using the same dynamic laws, which are defined as follows:

$$\dot{k}_{1i}(t) = \begin{cases} \omega_i\sqrt{\frac{\varsigma_i}{2}} & \text{if } \sigma \neq 0 \\ 0 & \text{if} \sigma = 0 \end{cases} \tag{40}$$

$$k_{2i}(t) = 2\epsilon_i k_{1i}(t) + \beta_i + 4\epsilon_i^2 \tag{41}$$

where $\omega_i$, $\varsigma_i$, $\beta_i$, $\overline{\eta}_i$ and $\epsilon_i$ are arbitrary positive constants for $i = \overline{1,6}$. The adaptive STA control law is expressed by (38) with adaptive gains (40)—(41). For the tuning process, we utilized the previously proposed tuning algorithm Guerrero, Torres, Creuze and Chemori (2019a).

Finally, PID control, another popular control technique widely employed in ROV operations, was considered. The PID control law is defined as follows (further details are available in the literature Campos, Chemori, Creuze, Torres and Lozano (2017)):

$$\tau_\eta = \hat{M}_\eta\ddot{\eta}_d + \hat{C}_\eta\dot{\eta}_d + \hat{D}_\eta\dot{\eta}_d - K_p e(t) - K_i\int e(\tau)d\tau - K_d\dot{e}(t) \tag{42}$$

where $\tau_\eta$ denotes the control input signal. The vectors $\dot{\eta}_d$ and $\ddot{\eta}_d$ denote the first and second time derivatives of the desired pose vector of the robot, respectively. $\hat{M}_\eta$, $\hat{C}_\eta$, and $\hat{D}_\eta$ are the estimates of the matrices $M$, $C$, and $D$, respectively. The feedback gains are defined as $K_p, K_i, K_d \in \mathbb{R}^{6\times6}$. The tracking errors and their time derivatives are denoted as $e(t)$ and $\dot{e}(t)$, respectively.
In the tuning process for the PID, the feedback gains were tuned heuristically when the robot simultaneously tracked the trajectory in depth and yaw dynamics. We selected the best gains for this controller without considering external disturbances during the experiment.

## 5.2. Real-Time Experimental Scenarios

To validate the effectiveness and robustness of the proposed control scheme, it was tested under different conditions; as a result, the following scenarios were considered:

1. The nominal scenario, wherein we tested the controller's capability for trajectory tracking in depth and yaw dynamics without considering external disturbances.
2. A parametric uncertainty scenario, wherein we modified the hydrodynamic parameters of the underwater vehicle to test the controller's robustness. To this end, we attached a floater and a rigid plastic sheet to the vehicle's body, as illustrated in Figure 4.
3. A sudden online mass variation scenario, wherein we simulated the robot carrying and then releasing an object. To realize this scenario, we attached a 335-g mass through a 60-cm rope to the body of the vehicle, as illustrated in Figure 5.
4. An external disturbance scenario, wherein we tested the controller's robustness towards disturbances applied to the robot while tracking the desired trajectory. We realized this scenario by pushing the robot several times with a long stick, as illustrated in Figure 6.

**Table 1**
Main Features of the underwater vehicle

| | |
|---|---|
| Mass | 28 $kg$ |
| Buoyancy | 9 $N$ |
| Dimensions | $75 \times 55 \times 45$ cm |
| Maximal depth | 100m |
| Thrusters | 6 Seabotix BTD150 |
| Power | 24V - 600 W |
| Attitude Sensor | InvenSense MPU-6000 MEMS 3-axis gyro and accelerometer<br>3-axis I2C magnetometer HMC-5883L<br>Atmega328 microprocessor |
| Camera | Pacific Co. VPC-895A<br>CCD1/3 PAL-25-fps |
| Depth sensor | Pressure Sensor MS5803-02BA |
| Sampling period | 50 ms |
| Surface computer | Dell Latitude E6230- Intel Core i7 -2.9 GHz<br>Windows 10 Professional 64 bits<br>Microsoft Visual C++ 2015 |
| Tether length | 30 m |

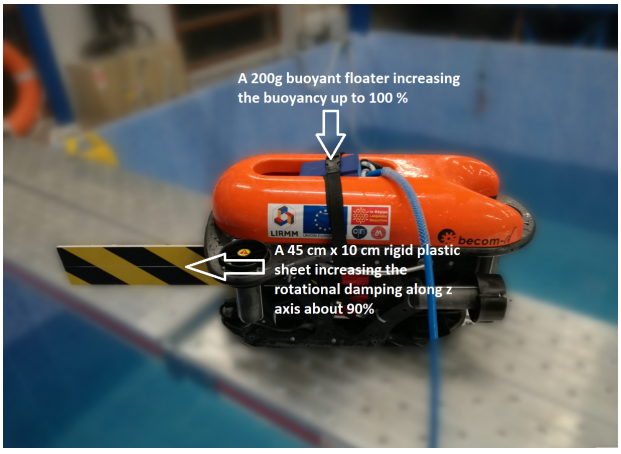


**Figure 4:** Configuration for scenario 2. We modified the vehicle's buoyancy by adding a 200 g floater to increase it up to 100%. A rigid plastic sheet of dimensions 45 cm × 10 cm was also attached to the robot's body to increase the rotational damping along the z-axis by approximately 90%.

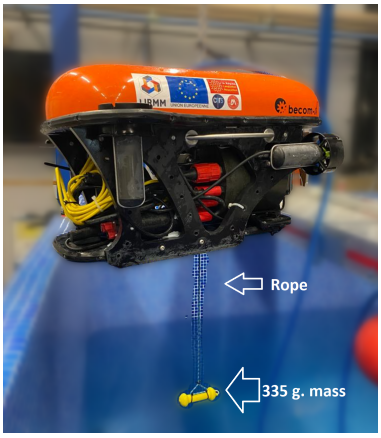


**Figure 5:** Configuration for scenario 2. We modified the vehicle's buoyancy by adding a 200 g floater to increase it up to 100%. A rigid plastic sheet of dimensions 45 cm × 10 cm was added to the robot's body to increase the rotational damping along the z-axis by approximately 90%.

### 5.3. Performance Criteria

To compare the performance of the trajectory tracking task for all controllers fairly, we propose the following criteria:

- The root mean square error (RMSE), which is defined as follows:

$$RMSE = \sqrt{\frac{1}{T_f}\int_0^{T_f} \|e(t)\|^2 dt} \tag{43}$$

  where $T_f$ denotes the duration of the experimental test, and $e(t)$ is the tracking error.

- To quantify the energy consumption, we propose to use the integral of the control input index (INT), which is defined as

$$INT = \int_{t_i}^{t_f} |\tau(t)| dt \tag{44}$$

  where $\tau(t)$ is the vector of position/attitude control input, $t_i$ and $t_f$ are the initial and final times of the experiment, respectively.

### 5.4. Scenario 1: The nominal case

In this scenario, the robot is controlled to simultaneously track a desired trajectory in depth and yaw DOFs; no external disturbances or parametric uncertainties are considered. The results obtained in this scenario are shown in Figure 7.

In the upper part of this figure, the robot simultaneously tracks the reference trajectory (black dashed line) in terms of depth and yaw. The left part of the graph shows the results of the depth tracking; evidently, the Sat-STA (red solid line) performs better than the nominal STA (blue solid line), PID (yellow solid line), and adaptive STA (green solid line). In addition, as evident from the yaw trajectory tracking, all controllers exhibited similar behavior at the beginning of the experiment. However, the Sat-STA controller showed a better tracking error than the STA controller, adaptive STA, and PID at the end of the test. The tracking errors for all the controllers are shown in the middle graphs of Figure 7. Further, the Sat-STA outperforms the nominal STA, adaptive STA, and PID, and the errors converge toward the origin. Finally, the control input signals for each controller are shown in the bottom graphs of Figure 7.

Notably, the Sat-STA generally outperforms the STA, adaptive STA, and PID in this nominal scenario, which is also numerically confirmed on the basis of the RMSE in the first row of Table 2. As evident from the table, the RMSE for the proposed saturated controller is smaller than those for the nominal STA, adaptive STA, and PID controllers. From

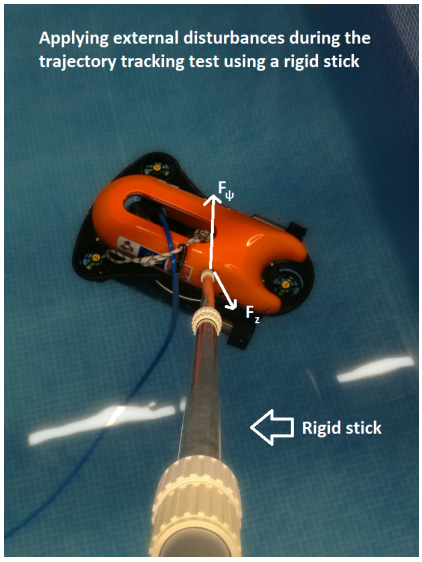


**Figure 6:** Configuration for scenario 4. We applied external disturbances while the robot tracks a trajectory in depth and yaw dynamics. Both dynamics (depth and yaw) were simultaneously disturbed.

an energy consumption perspective, it is expected that the Sat-STA scheme requires slightly more energy than the other controllers, which is confirmed through the reported values of the INT performance criterion summarized in the first row of Table 3.

### 5.5. Scenario 2: Robustness towards parametric uncertainties

In this scenario, we attached a rigid plastic sheet with dimensions of 45 cm × 10 cm to the ROV's body to increase the rotational damping along the z-axis by approximately 90%, resulting in a modified damping matrix $D_\eta(\cdot)$ in the dynamic model (4). Additionally, a floater was attached to the body of the robot to increase its buoyancy by up to 100%. Mathematically, this is equivalent to modifying the vector $g(\cdot)$ in (4).

The trajectory tracking results for this scenario are depicted in Figure 8. The upper-left part of this figure shows the plot of the trajectory tracking for the depth dynamics. The proposed controller (red solid line) exhibits a better tracking performance than does the STA nominal design (blue solid line), adaptive STA (green solid line), and PID (yellow solid line) when the robot tracks the desired trajectory in depth (black dashed line). As evident from the first 15 s of the experiment, the nominal STA has a significant tracking error compared with the proposed saturated controller; this implies that the nominal STA requires further effort to compensate for the added parametric uncertainties. Moreover, the adaptive STA control requires some time to auto-tune its gains. This effect is evident at the beginning of the test, starting with a large tracking error, which is then reduced when the gains are automatically increased. However, the PID control shows a constant tracking error during the first 40 s of the experiment, and the tracking error tended to be continuously reduced until the end of the test. Trajectory tracking for yaw dynamics is depicted in the upper-right part of Figure 8. Evidently, the Sat-STA controller performs better than the nominal STA, adaptive STA, and PID. The time evolutions of the trajectory tracking errors for both dynamics are plotted in the middle graphs of Figure 8. Both plots confirm that the proposed controller outperforms the nominal STA, adaptive STA, and PID. Finally, the evolutions of the control inputs for both dynamics are plotted in the bottom of Figure 8.

Regarding the performance criteria, the RMSE metric values for this case are summarized in the second row of Table 2. Evidently, the proposed Sat-STA outperforms the nominal STA, adaptive STA, and PID approaches, confirming the observations made previously. From the perspective of energy consumption, the STA controller requires more effort to counteract the added parametric uncertainties, as shown in the second row of Table 3.

### 5.6. Scenario 3: Robustness towards payload change

In this scenario, we simulated a varying payload while tracking the desired trajectory in depth dynamics by attaching a $335 - g$ mass to the body of the robot by using a 60cm rope, as illustrated in Figure 5. The experiment began with the robot at rest on the surface. However, because of the added weight, the robot began the test at approximately 0.3 $m$ of depth. As time progresses, the time-varying desired depth increases, and when the robot depth reaches $z_d = 0.45\ m$, the payload touches the pool floor, resulting in a sudden change in the mass carried by the vehicle. After approximately 20 s, the desired depth of the vehicle changed, and the robot moves upward to $z_d = 0.25\ m$, resulting in a change in payload from 0 to 330 g. The AUV remained at the desired depth until the end of the experiment. In this scenario, the yaw dynamics were not affected.

The trajectory tracking results for this scenario are depicted in Figure 9. The top-left part of the figure shows the results of trajectory tracking in depth (black dashed line). We compared the tracking performance of the STA (blue solid line), adaptive STA (green solid line), PID (yellow solid line), and proposed saturated controller (red solid line). The results indicate that the initial depth of the robot is approximately 0.3 $m$ because of the added weight. The vehicle attempts to follow the reference trajectory, and it is evident that the saturated controller has a better tracking error than does the nominal STA, adaptive STA, and PID. Next, when the desired trajectory reaches $z_d = 0.45\ m$, the weight touches the floor of the pool, causing oscillations near the desired point for the STA and PID controllers. However, for the proposed Sat-STA and adaptive STA, this effect was not apparent. After remaining at 0.50 $m$ for 20 s, the desired position changed with time, and when the vehicle moves upward to $z_d = 0.25\ m$, the robot again carried the weight at 35 s. When the payload is acting on the robot, the dynamics of the vehicle change, and it can be observed that the controllers attempt to compensate for this additional

weight. The PID controller showed a constant tracking error during testing. The trajectory tracking results for the yaw dynamics are shown in the top-right graphs in Figure 9. Evidently, all controllers exhibit similar performances. The trajectory tracking errors are shown in the middle graphs of Figure 9. The errors for the proposed saturated controller were smaller than those for the nominal STA, adaptive STA, and PID designs when depth tracking was considered. The trajectory tracking errors for yaw are shown in the middle-right part of the figure. Finally, at the bottom graphs of Figure 9, the time evolutions of the control inputs for both dynamics are plotted.

The RMSE values for the scenario are listed in the third row of Table 2. The Sat-STA outperforms the nominal STA, adaptive STA, and PID controllers because it exhibits smaller RMSE values for both dynamics (i.e., depth and yaw). However, in terms of energy consumption, as expected, the proposed controller exhibits slightly larger values than do the nominal STA, adaptive STA, and PID designs, as shown in the third row of Table 3.

### 5.7. Scenario 4: External disturbance rejection

In this scenario, the robot tracked the same trajectories as in the nominal case under the same operating conditions. However, to evaluate the performance of the proposed controller in terms of the external disturbance rejection, we manually applied several perturbations with a long stick during the test, as illustrated in Figure 6. The considered disturbances were generated by a human operator; therefore, we did not compare the proposed controller with the STA nominal design because it is impossible to guarantee the repeatability of those disturbances.

The top graphs of Figure 10 show the trajectory tracking for depth (left) and yaw (right). We manually applied disturbances six times during this test; this is indicated by the peaks in the graphs. The controller can manage this disturbance because after applying the perturbation to the robot; it takes only a few seconds to recover the trajectory, as shown in the left part of the figure. The first three disturbances applied to the robot mainly focused on the depth dynamics. In contrast, both dynamics were affected by the last three external disturbances. Even when the yaw dynamics are disturbed, the controlled vehicle can manage the disturbance and shows a fast recovery after each impact. The middle of Figure 10 shows the plot of the time evolution of the tracking errors for this test. At the bottom of the figure, the time evolution of the generated control effort for each controller is shown.

Finally, the fourth row of Table 2 presents the RMSE values for both dynamics. In addition, the fourth row of Table 3 lists the energy consumptions during this scenario.

## 6. Conclusion and future works

In this study, we demonstrated a novel approach for enhancing the trajectory-following capabilities of AUVs by developing a saturated STA-based controller. Based on the classical STA, the proposed controller incorporates a saturation function, mitigating the potential for the windup effect inherent in such algorithms. This adaptation becomes crucial in handling situations wherein the control input saturation and integral term of the super-twisting algorithm could otherwise compromise performance.

The extension of the controller to MIMO systems, specifically tailored for the dynamics of AUVs, underscores its versatility and applicability across complex operational scenarios. To substantiate the effectiveness and reliability of the proposed control scheme, a rigorous Lyapunov-based stability analysis is presented.

Furthermore, a comprehensive real-time experimental study, performed for validating the proposed saturated STA, is detailed. The experiments entailed subjecting the controller to four distinct scenarios under various operating conditions. The robustness and efficacy of the algorithm in facilitating precise trajectory tracking for AUVs over other robust techniques such as the nominal STA, adaptive STA, and PID controller are demonstrated. The results not only confirm the theoretical foundations established through the stability analysis but also showcase the practical utility of the proposed controller in real-world applications. Its potential contribution to the advancement of AUV control systems is thus highlighted. In future research, we intend to design an adaptive saturated STA controller.

## Acknowledgements

This work was supported by the French Occitanie Region within the framework of the project “Défi-clé Robotique Centrée sur l’Humain" under Grant N° 21034741.

## CRediT authorship contribution statement

**Jesús Guerrero:** Conceptualization of this study, Methodology, Software, Data collection, Original draft preparation. **Ahmed Chemori:** Software, Writing, Data Collection - Original draft preparation. **Vincent Creuze:** Software, Writing - Original draft preparation. **Jorge Torres:** Writing, Original and final draft preparation. **Eduardo Campos:** Writing, Original and final draft preparation.

## References

Campos, E., Chemori, A., Creuze, V., Torres, J., Lozano, R., 2017. Saturation based nonlinear depth and yaw control of underwater vehicles with Stability analyses and real-time experiments. Mechatronics 45, 49–59.

Castillo, I., Steinberger, M., Fridman, L., Moreno, J.A., Horn, M., 2021. A lyapunov based saturated super-twisting algorithm. Emerging Trends in Sliding mode control: Theory and Application, 47–68.

Fossen, T.I., 1999. Guidance and control of ocean vehicles. University of Trondheim, Norway, Printed by John Wiley & Sons, Chichester, England, ISBN: 0 471 94113 1, Doctors Thesis.

Fossen, T.I., 2011. Handbook of Marine-Craft Hydrodynamics and Motion Control. John Wiley & Sons.

Golkani, M.A., Koch, S., Reichhartinger, M., Horn, M., 2018. A novel saturated super-twisting algorithm. Systems & Control Letters, 119, 52–56.

Guerrero, J., Torres, J., Antonio, E., Campos, E., 2018. Autonomous under- Robust Water Vehicle Path Tracking: Generalized Supertwisting Algorithm and block backstepping controllers. Journal of Control Engineering Applied Informatics 20, 51–63.

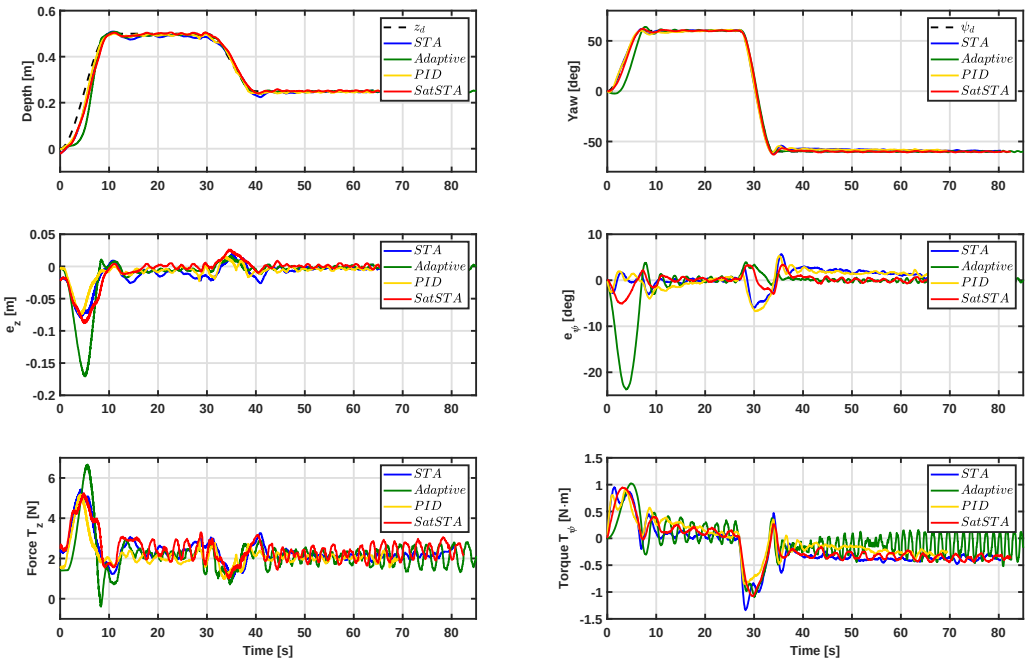


**Figure 7:** nominal case. The robot tracks a desired trajectory (black dashed line) in depth and yaw dynamics (top). The results for the proposed saturated controller (red solid line), nominal STA (solid blue line), adaptive STA (green solid line), and PID (solid yellow line) are shown. The tracking errors of both dynamics are shown in the middle graphs. At the bottom, the force and torque for depth and yaw dynamics are plotted.

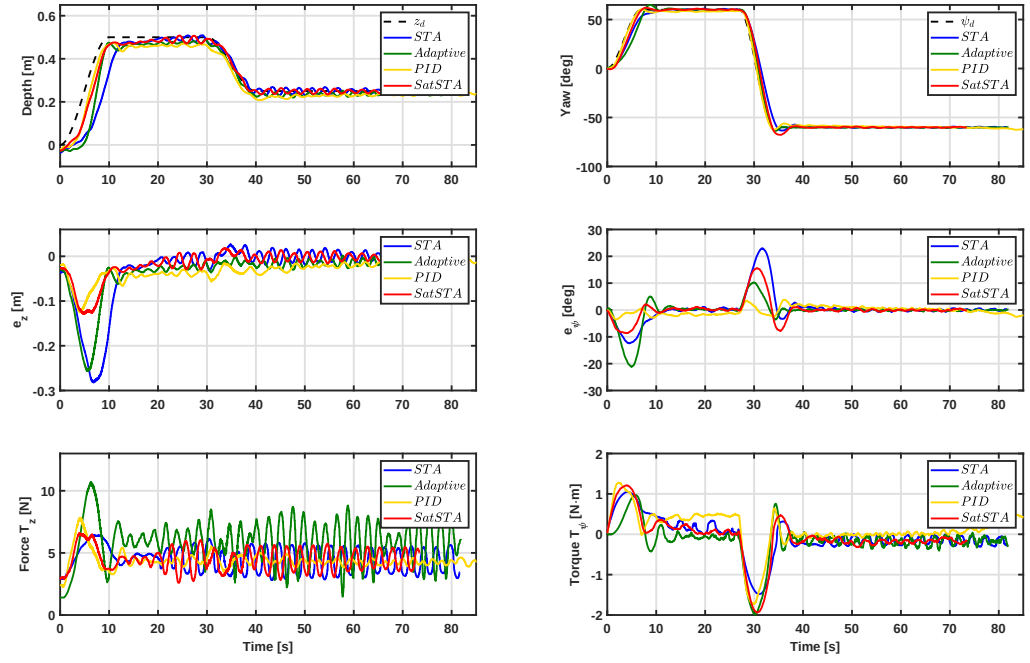


**Figure 8:** Robustness towards parametric uncertainties. Experimental results of the trajectory tracking in depth and yaw; the desired trajectory (black dashed line), nominal STA (solid blue line), proposed saturated STA controller (solid red line), adaptive STA (green solid line), and PID (yellow solid line) are shown.

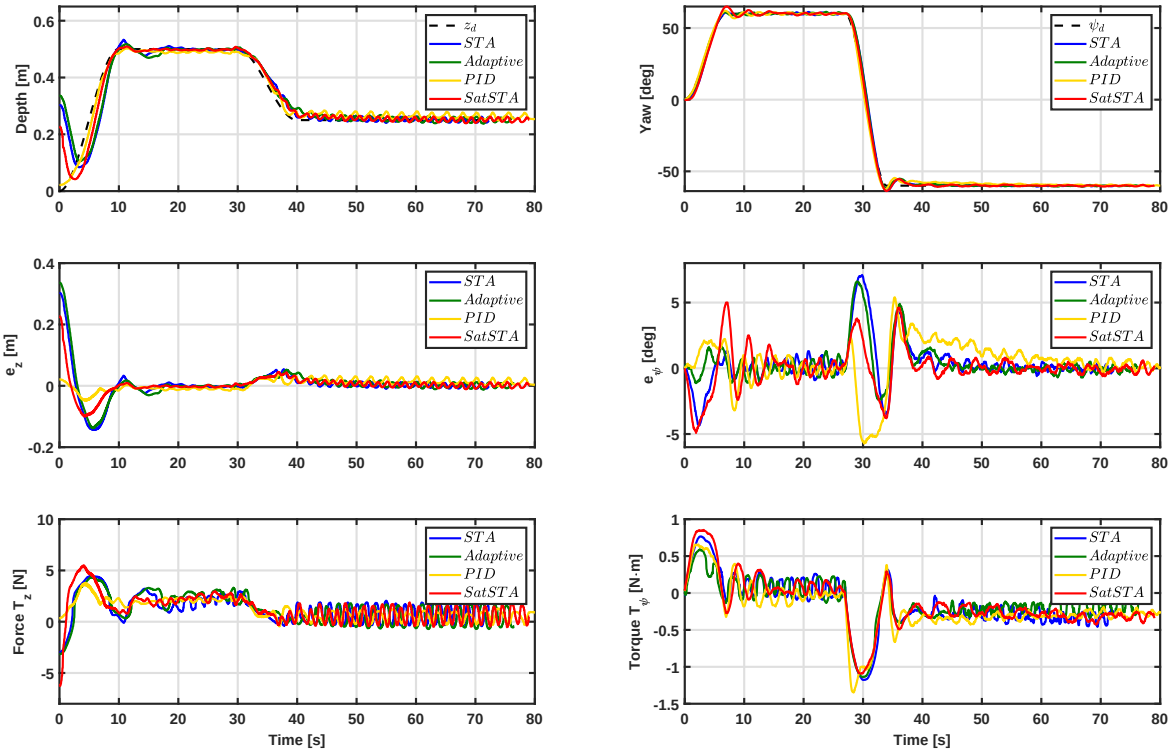


**Figure 9:** Robustness towards sudden mass change. Experimental results of the trajectory tracking in depth and yaw; the desired trajectory (black dashed line), nominal STA (solid blue line), adaptive STA (green solid line), proposed saturated controller (solid red line), and PID (solid yellow line) are shown.

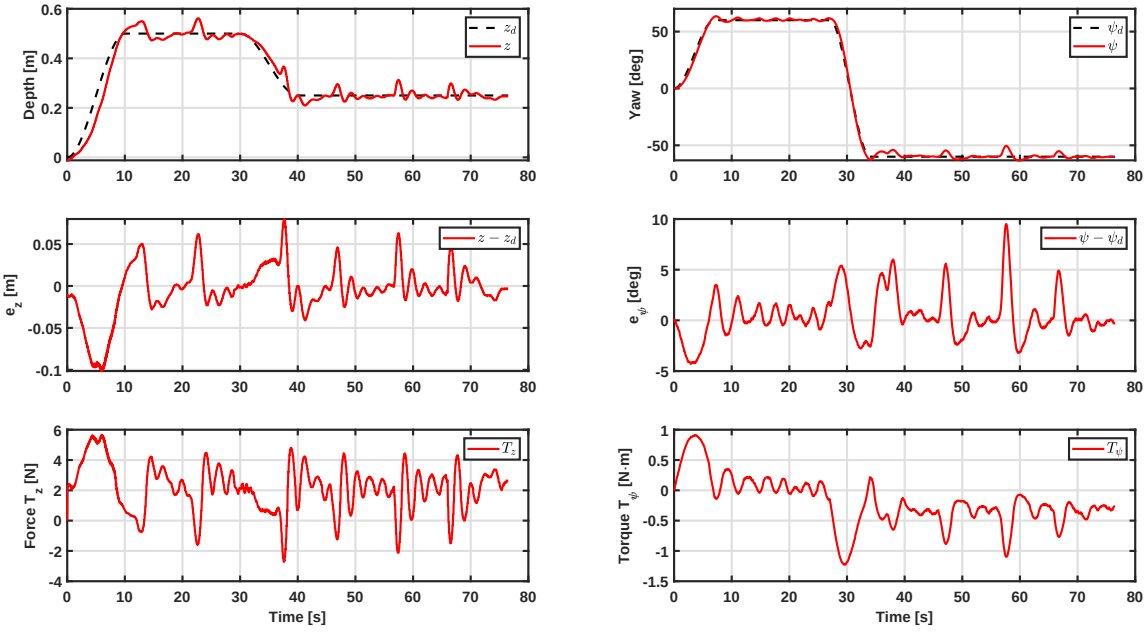


**Figure 10:** Robustness towards external disturbance rejection. Experimental results of the trajectory tracking in depth and yaw; the desired trajectory (black dashed line) and the proposed saturated controller (solid red line) are shown.

**Table 2**
RMSE comparison criteria for STA, Sat-STA, adaptive STA and nominal PID

| | STA | | Sat-STA | | Adaptive STA | | PID | |
|---|---|---|---|---|---|---|---|---|
| Case | z (m) | $\psi$ (deg) | z (m) | $\psi$ (deg) | z (m) | $\psi$ (deg) | z (m) | $\psi$ (deg) |
| 1 | 0.0099 | 0.5592 | **0.0051** | **0.0438** | 0.0084 | 0.8943 | 0.0083 | 0.2964 |
| 2 | 0.0261 | 0.4648 | **0.0166** | **0.1208** | 0.0333 | 0.5274 | 0.0319 | 0.2747 |
| 3 | 0.0031 | 0.3723 | **0.0024** | **0.0374** | 0.0060 | 0.3985 | 0.0058 | 0.3607 |
| 4 | – | – | **0.0044** | **0.4067** | – | – | – | – |

**Table 3**
Energy consumption comparison criteria through the INT metric for STA, the Sat-STA, the adaptive STA, and the nominal PID.

| | STA | | Sat-STA | | Adaptive STA | | PID | |
|---|---|---|---|---|---|---|---|---|
| Case | z (m) | $\psi$ (deg) | z (m) | $\psi$ (deg) | z (m) | $\psi$ (deg) | z (m) | $\psi$ (deg) |
| 1 | 3814 | 566 | 4084 | 553 | 4250 | 490 | 2980 | 388 |
| 2 | 7333 | 513 | 6585 | 494 | 9662 | 459 | 7605 | 540 |
| 3 | 2101 | 445 | 2323 | 474 | 2313 | 375 | 2104 | 567 |
| 4 | – | – | 3538 | 542 | – | – | – | – |


Guerrero, J., Torres, J., Creuze, V., Chemori, A., 2019a. Trajectory tracking for autonomous underwater vehicles: an adaptive approach. Ocean Engineering 172, 511–522.

Guerrero, J., Torres, J., Creuze, V., Chemori, A., Campos, E., 2019b. Saturation-Based Nonlinear PID Control for Underwater Vehicles: Design Stability analyses and experiments. Mechatronics 61, 96–105.

Guerrero, J., Chemori, A., Torres, J., Creuze, V. 2023. Time-delay high-order sliding mode control for trajectory tracking of autonomous underwater vehicles under disturbances. Ocean Engineering, 268, 113375.

Herman, P., 2009. Decoupled pd set-point controller for underwater vehicles. Ocean Engineering 36: 529–534.

Levant, A., 1993. Sliding order and sliding accuracy in the sliding mode control. International Journal of control 58, 1247–1263.

Li, B., Gao, X., Huang, H., Yang, H., 2024. Improved adaptive twisting sliding mode control for trajectory tracking of AUV subject to uncertainty. Ocean Engineering, 297, 116204.

Li, X., Wen, H., Cao, J., Yao, B., Lian, L., Mao, Z. 2023. Design of adaptive sliding-mode controller combined with pseudo-inverse-based thruster allocator for ROV with variable coefficients. Ocean Engineering, 286, 115530.

Liu, L., Zhang, L., Pan, G., Zhang, S., 2022. Robust yaw control of autonomous underwater vehicles based on a fractional-order pid controller. Ocean Engineering 257: 111493.

Maalouf, D., Creuze, V. and Chemori, A., "A Novel Application of Multivariable L1 Adaptive Control: From Design to Real-Time Implementation on an Underwater vehicle", 2012 IEEE/RSJ International Conference on Intelligent Robots and Systems, Vilamoura-Algarve, Portugal, 2012.

Manzanilla, A., Ibarra, E., Salazar, S., Zamora, Á.E., Lozano, R., Munoz, F., 2021. Supertwisting integral sliding mode control of trajectory Tracking unmanned underwater vehicles. Ocean Engineering 234, 109164.

Martínez-Fuentes, C.A., Seeber, R., Fridman, L., Moreno, J.A., 2020. Saturated lipschitz continuous sliding mode controller for perturbed systems with uncertain control coefficients. IEEE Transactions on Automatic Control 66, 3885–3891.

Orlov, Y. V. (2008). Discontinuous systems: Lyapunov analysis and robust synthesis under uncertain conditions. Springer Science & Business Media.

Qiao, L., Zhang, W. (2019). Trajectory tracking control of AUVs via adaptive fast nonsingular integral terminal sliding mode control. IEEE Transactions on Industrial Informatics, 16(2), 1248-1258.

Sarhadi, P., Noei, A.R., Khosravi, A., 2016. Model reference adaptive pid Control using an anti-windup compensator for autonomous underwater operation vehicle. Robotics and Autonomous Systems, 83, 87–93.

Seeber, R., Reichhartinger, M., 2020. Conditioned super-twisting algorithm for systems with a saturated control action. Automatica 116: 108921.

Shojaei, K., 2022. Neural network feedback linearization target tracking Control of underactuated autonomous underwater vehicles with guar anteed performance. Ocean Engineering 258: 111827.

Tijjani, A.S., Chemori, A., Ali, S.A., Creuze, V., 2022a. Continuous–discrete observation-based robust underwater tracking control Vehicles: design, stability analysis, and experiments. IEEE Transactions on Control Systems Technology, 1–16doi:10.1109/TCST.2022.3224321.

Tijjani, A.S., Chemori, A., Creuze, V., 2020. Robust adaptive tracking control trol of underwater vehicles: design, stability analysis, and experiments. IEEE/ASME Transactions on Mechatronics.

Tijjani, A.S., Chemori, A., Creuze, V., 2022b. A survey on tracking Control of Unmanned Underwater Vehicles: Experiment-based Approach. Annual Reviews in Control doi:https://doi.org/10.1016/j.arcontrol.2022.07.001.

Xiang, X., Yu, C., Lapierre, L., Zhang, J., Zhang, Q., 2018. Survey of fuzzy-logic-based guidance and control of marine surface vehicles and underwater vehicles. International Journal of Fuzzy Systems 20, 572–586.

Xu, Z., Haroutunian, M., Murphy, A. J., Neasham, J., Norman, R. 2020. Comparison of functional control strategies for underwater vehicles: theories, simulations, and experiments. Ocean Engineering, 215, 107822.

Yan, Z., Gong, P., Zhang, W., Wu, W. 2020. Model predictive control of autonomous underwater vehicles for trajectory tracking with external disturbances. Ocean Engineering, 217, 107884.

Yan, Z., Yan, J., Cai, S., Yu, Y., Wu, Y. 2023. Robust MPC-based trajectory Tracking of autonomous underwater vehicles with Model Uncertainties Ocean Engineering, 286, 115617.

Zhong, Y., Yu, C., Wang, R., Liu, C., Lian, L. (2022). Adaptive depth tracking of underwater vehicles considering actuator saturation: Theory, simulation, and experiment. Ocean Engineering, 265, 112517.